Application of Frequency-dependent Traveltime Tomography and Full Waveform Inversion to Realistic Near-surface Seismic Refraction Data

Jianxiong Chen and Colin A. Zelt
Department of Earth Science, 6100 Main Street, MS-126, Rice University, Houston, Texas 77005
Email: jc33@rice.edu; czelt@rice.edu

ABSTRACT

We present a synthetic test that uses a workflow consisting of a new frequency-dependent traveltime tomography (FDTT) method to provide a starting model for full waveform inversion (FWI) for near-surface seismic velocity estimation from refraction data. Commonly used ray-theory-based traveltime tomography methods may not be valid in the near surface given the likelihood of relatively large seismic wavelengths compared to the length scales of heterogeneities that are possible in the near surface. FDTT makes use of the frequency content in the seismic waves in both the forward and inverse modeling steps. In this application to a near-surface benchmark model, the results show that FDTT can better recover the magnitude of velocity anomalies than infinite frequency (ray-theory) traveltime tomography (IFTT). FWI can fail by converging to a local minimum when there is an absence of sufficiently low frequency data and an accurate starting model, either of which, if present, can provide long-wavelength constraints on the inverted velocity model. Both IFTT and FDTT models can serve as adequate starting models for FWI. However, FWI produces significantly better results starting from the FDTT model as compared to the IFTT model when low frequency data are not available. The final FWI models provide wavelength-scale structures allowing for direct geologic interpretation from the velocity model itself, demonstrating the effectiveness of FDTT and FWI in near-surface studies given the modest experiment and data requirements of refraction surveys.

Introduction

Seismic methods, including tomography, are used to address a number of near-surface environmental, engineering, archeological, neotectonic and resource exploration problems (Steeples, 2001; Pelton, 2005). Ray theory is commonly assumed to analyze the arrival times of seismic waves for velocity model estimation (*e.g.*, Zhao and Xu, 2010; Ramachandran *et al.*, 2011; Baumann-Wilke *et al.*, 2012). Compared with global-scale or crustal-scale studies, where the size of anomalies is typically much larger than that of the seismic wavelength, in the near surface (<100-m depth), the size of anomalies is often comparable with or smaller than the seismic wavelength (*e.g.*, Gao *et al.*, 2007), invalidating the infinite frequency assumption of ray theory.

Zelt and Chen (2016) present a form of frequency-dependent traveltime tomography (FDTT) that takes frequency content into consideration in both the forward and inverse modeling steps. It represents a small modification to ray theory in which the velocity model is pre-smoothed and the width of the sensitivity kernels is extended, both of which are determined by the local seismic wavelength (Zelt and Chen, 2016). The advantage of FDTT over ray-theory-based infinite frequency traveltime tomography (IFTT) is more significant for near-surface data because of the relatively longer seismic wavelengths and smaller heterogeneities. Applications of FDTT to realistic synthetic and real data reveal better results than IFTT, especially in terms of recovery of the true magnitude of velocity anomalies (Zelt and Chen, 2016). As a result, the model obtained from FDTT has the potential to provide more accurate information for geologic interpretation and can be used as a more effective starting model for full waveform inversion (FWI) (Pratt, 1999).

In this paper, we test FDTT and FWI using a synthetic dataset generated from a realistic near-surface velocity model (Fig. 1(a)) that was used previously in a blind test of first-arrival-time inversion and tomography methods (Zelt *et al.*, 2013). The estimated velocity models from ten participants in the blind test using eight different inversion algorithms are generally consistent in their large-scale (>wavelength) features, but show only smooth expressions of the true model's key features (Fig. 1(b)). The deeper part of the model (>35 m) is not

JEEG, March 2016, Volume 21, Issue 1, pp. 1–11
DOI: 10.2113/JEEG21.1.1

as well resolved as the shallower part given the ray coverage (Fig. 1(c)). Since the original release of the traveltime data and the velocity model in the blind test in 2011, there have been studies (*e.g.*, Rohdewald, 2014; Stoyer, 2012) using different methods for analyzing the traveltimes to improve the inverted model resolution.

The primary goal of this paper is to serve as a follow-up and an extension to all the previous discussions on this realistic synthetic model by generating and inverting waveform data. The focus of this paper is to test the ability of the combination of FDTT and FWI to characterize the large-scale and wavelength-scale structures in near-surface studies, compared to only characterizing the large-scale structures as shown by the previous studies that only used traveltime data.

Previous applications of FWI (*e.g.*, Smithyman *et al.*, 2009; Adamczyk *et al.*, 2014) commonly present synthetic tests as a way of assessing FWI. These tests use accurate background velocity models as the starting model for FWI to recover velocity anomalies with regular shapes (*e.g.*, a checkerboard model). Using an accurate background model as the starting model means that the researchers assume the suitability of using a model from traveltime tomography (TT) as the starting model for FWI.

Brenders and Pratt (2007a) presented blind tests for a realistic crustal-scale model using a workflow including TT to obtain the starting model for FWI. In a following paper, Brenders and Pratt (2007b) tested the influence of adjusting different input parameters on FWI, but they did not test the influence of using different starting models for FWI.

This paper uses the realistic synthetic near-surface velocity model in Zelt *et al.* (2013) and extends the discussions by incorporating waveform data and using a combined workflow of FDTT and FWI. The results and extended discussions in this paper 1) confirm the suitability of using IFTT/FDTT to provide the starting model for FWI, 2) demonstrate the ability of FDTT to produce a more accurate starting velocity model for FWI to mitigate the lack of low frequency data, 3) show the improvement in model estimation using a combined strategy of FDTT and FWI, and 4) promote the use of FDTT and FWI in near-surface studies given the modest experiment and data requirements of refraction surveys over conventional reflection surveys.

Model and Data

The true velocity model (Fig. 1(a)) represents a geologic setting consisting of unconsolidated sediment overlying faulted bedrock (Zelt *et al.*, 2013). The key features and potential targets for the seismic inversions in this model are: 1) a thin low-velocity layer in the sediments

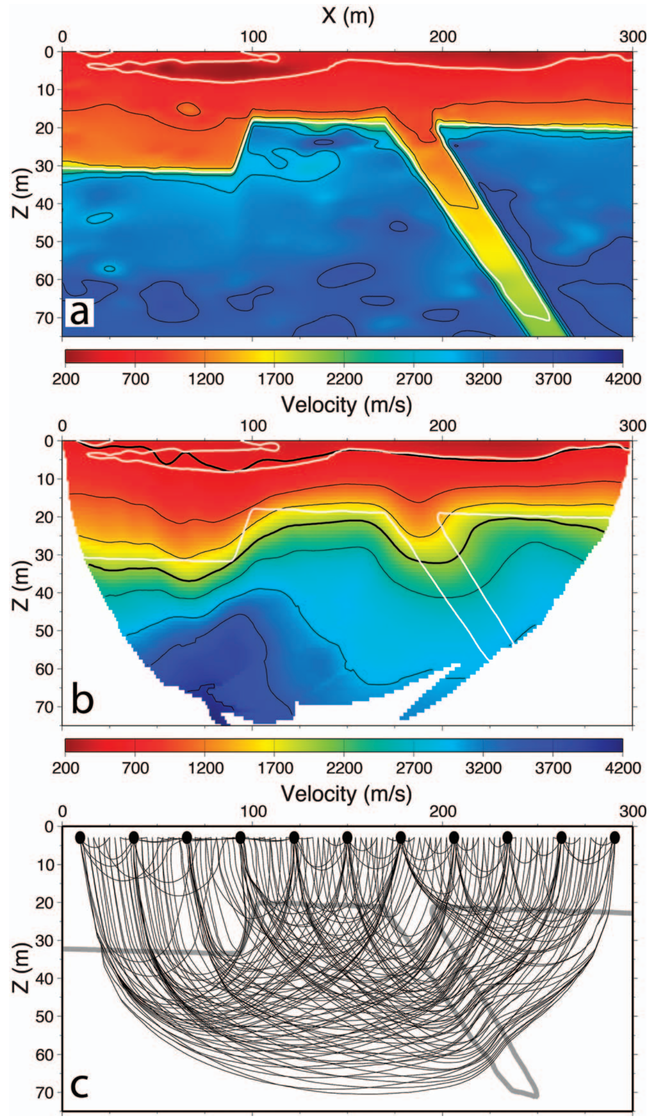

Figure 1. a) True model. White contours correspond to 500 m/s and 2,000 m/s. b) Average of 14 estimated models from. Zelt *et al.* (2013). Thick black contours correspond to 500 m/s and 2,000 m/s. White contours are from true model for comparison. The blank area lacks ray coverage. c) Ray paths through true model. In Zelt *et. al.* (2013), 101 shots and 100 receivers were used. For clarity, every 5th ray from every 10th shot is shown (Zelt *et. al.*, 2013). Vertical exaggeration is two.

~5-m deep between 12.5 m and 112.5 m lateral position, 2) a steep bedrock offset of ~12 m centered at 95 m lateral position, and 3) a steeply dipping (~35°) low-velocity fault zone in the bedrock centered at 185 m lateral position and 20-m depth. The surface topography is flat.

For the blind test presented in Zelt *et al.* (2013), the inverted data were traveltimes calculated using wavelength-dependent velocity smoothing (Zelt and Chen, 2016) corresponding to 100 Hz for 101 shots and

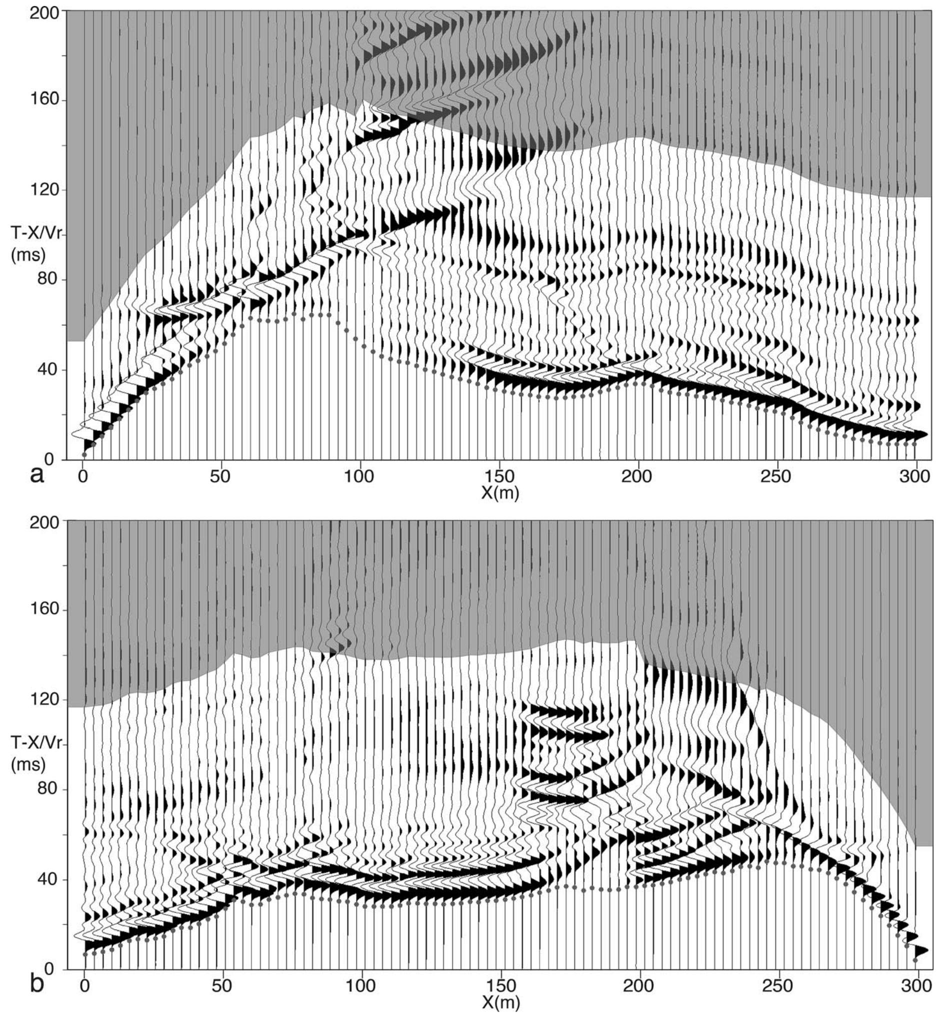

Figure 2. Representative synthetic acoustic seismograms from two end shots. The grey dots indicate the manually picked first arrival times. A reducing velocity (Vr) of 2,000 m/s is used to amplify subtle changes in the apparent velocities of both the near- and far-offset traces within the smallest possible time window. The seismic waveforms in the shaded areas were not used for waveform inversion as a result of the time window excluding later arrivals.

100 receivers. In this paper, waveform data are needed for FWI, but not available from the blind test. Acoustic waves are simulated in the frequency domain (Pratt, 1999), transformed to the time domain for manual first-arrival picking as the input for traveltime tomography (Fig. 2), and later time-windowed (see Methods section) as a realistic processing step before transforming back to the frequency domain for waveform inversion. In this study, first-arrival picks and waveforms from 25 sources are used as compared to calculated times from 101 sources in Zelt *et al.* (2013); the smaller number of sources corresponds to a more realistic seismic experiment in terms of field work effort and cost. This reduction was also motivated by a result in Zelt *et al.* (2013) that also used a quarter of the shots to do the inversion and the resulting model fit the data from all 101 shots equally well. We have used 25 evenly spaced sources between 0 and 300 m, and 96 evenly spaced receivers between 1.5625 and 298.4375 m. The dominant frequency of the source wavelet is 80 Hz and the energy is down about 20 dB at 2 and 250 Hz. This spectrum is consistent with that of a realistic near-surface seismic survey (*e.g.*, Doll *et al.*, 1998).

Methods

This paper uses frequency-dependent traveltime tomography (Zelt and Chen, 2016) and full waveform inversion (Pratt *et al.*, 1998; Pratt, 1999) in a combined workflow where FDTT provides a starting model for FWI. Both methods solve a nonlinear inverse problem through a local decent method starting from an initial velocity model and iteratively updating it to reduce the differences between the modeled data and observed data.

FDTT inverts first-arrival times by calculating a frequency-dependent traveltime. FWI inverts the waveforms of the early arrivals by solving the acoustic wave equation in the frequency domain. In this section, we review the important components of the FDTT and FWI methodologies, but refer the readers to Zelt and Chen (2016), Pratt *et al.* (1998) and Pratt (1999) for more details. In the following equations, bold lowercase letters denote column vectors, and bold capitals are second-order matrices. The operations between the quantities are matrix multiplication unless otherwise explicitly stated.

Frequency-dependent Traveltime Tomography

The forward modeling component of FDTT consists of a wavefront-tracking algorithm that solves the 2-D eikonal equation on a square grid of velocity nodes using finite difference operators (Vidale, 1988), with modifications to allow for large velocity gradients (Hole and Zelt, 1995) and to take frequency into account (Zelt and Chen, 2016). The modification to calculate frequency-dependent traveltimes involves pre-smoothing the velocity model using a local cosine-squared, wavelength-dependent operator determined by the chosen frequency; this approach is called wavelength-dependent velocity smoothing (WDVS).

The observed data are the first arrivals that are picked corresponding to the onset of seismic energy of each seismic trace (Fig. 2) using a semi-automated scheme whereby a few picks were made interactively, and the intervening picks were determined automatically using a cross-correlation scheme (Zelt, 1999), resulting in a total of 2,400 picks. With noise-free synthetic data, as in this study, the onsets can be picked relatively accurately. As a result, the picks are interpreted as high frequency traveltimes, and thus the high end of the data spectrum is chosen for forward modeling during FDTT. We used 250 Hz corresponding to the frequency where the source wavelet energy is down ~20 dB. Each pick is assigned a 1 ms uncertainty, corresponding to a quarter of a period at 250 Hz, to be used in the inversion process for the stopping criteria based on an appropriate data misfit between the calculated first arrivals (modeled data) and the picked arrivals (observed data) (Zelt, 1999).

The inverse step of FDTT is the same as that used in IFTT as described by Zelt and Barton (1998), except the linear system of equations relating traveltime residuals and slowness perturbations is less sparse for FDTT because of the wavelength-dependent width of the sensitivity kernels (Zelt and Chen, 2016). For IFTT, the sensitivity kernels are nonzero only in the model cells along the ray path.

Given the strong lateral variations in the true model, a best-fit model with minimal lateral (2-D) structure was determined from the picked traveltimes using the Zelt and Smith (1992) algorithm to serve as the starting model for IFTT and FDTT (Fig. 3(b)). For both IFTT and FDTT, a regularized inversion algorithm is used to minimize the data misfit and model roughness to provide the smoothest model with a proper data misfit (Zelt and Barton, 1998). The objective function Φ of the regularized inversion is expressed as:

$$\Phi(\boldsymbol{m})=\delta\boldsymbol{t}^T \boldsymbol{C}_d^{-1}\,\delta\boldsymbol{t}+\lambda[\alpha(\boldsymbol{m}^T \boldsymbol{C}_h^{-1}\,\boldsymbol{m}+s_z\,\boldsymbol{m}^T \boldsymbol{C}_v^{-1}\,\boldsymbol{m}) +(1-\alpha)\,(\boldsymbol{m}-\boldsymbol{m}_0)^T\,(\boldsymbol{m}-\boldsymbol{m}_0)], \tag{1}$$

where $\boldsymbol{m}$ is the model vector; $\boldsymbol{m}_0$ is the starting model vector; $\delta\boldsymbol{t}$ is the traveltime data residual vector; $\boldsymbol{C}_d$ is the data covariance matrix; $\boldsymbol{C}_h$ and $\boldsymbol{C}_v$ are the horizontal and vertical roughness matrices, respectively; λ is the trade-off parameter that weighs the relative importance of data misfit and model regulations; s_z determines the relative importance of maintaining vertical versus horizontal model smoothness; and α weighs the relative importance of model smoothness and the absolute model perturbation. The superscript T represents transpose, and the superscript -1 represents matrix inverse. During inversions, s_z and α are fixed, λ starts with a relatively large free-parameter value and is decreased automatically during the iterations updating the velocity model to introduce large-scale structure first and fine-scale structure in later iterations. At the end, λ is adjusted to yield a final model that provides a normalized chi-squared misfit value of one, quantitatively indicating that the picked arrivals have been fit to within the assigned uncertainties (Zelt, 1999).

Frequency-domain Full Waveform Inversion

The forward modeling of FWI solves the isotropic, 2-D, visco-acoustic wave equation in the frequency domain that can be expressed as:

$$\boldsymbol{S}\boldsymbol{u}=\boldsymbol{f}, \tag{2}$$

where the complex impedance matrix $S = K-\omega^2 M + i\omega\boldsymbol{C}$ is a linear combination of the stiffness matrix $\boldsymbol{K}$, mass matrix $\boldsymbol{M}$, and damping matrix $\boldsymbol{C}$, and where ω is the angular frequency. The vector $\boldsymbol{f}$ represents the source signature, and the vector $\boldsymbol{u}$ represents the seismic wavefield to be calculated. Equation (2) can be expressed as $u = S^{-1}f$, and it is discretized by a finite-difference method and numerically solved by LU decomposition (Pratt *et al.*, 1998; Pratt 1999). An 80 Hz-dominant frequency Ricker wavelet is used as the source. The data are modeled from 2 to 400 Hz with a 2 Hz interval.

Pre-processing the data to account for the acoustic approximation is crucial for real data applications, for example, pre-inversion matching of the amplitude between the observed and modeled data (*e.g.*, Brenders and Pratt, 2007a; Ravaut *et al.*, 2004). It is not needed for the noise-free synthetic test in this paper since the

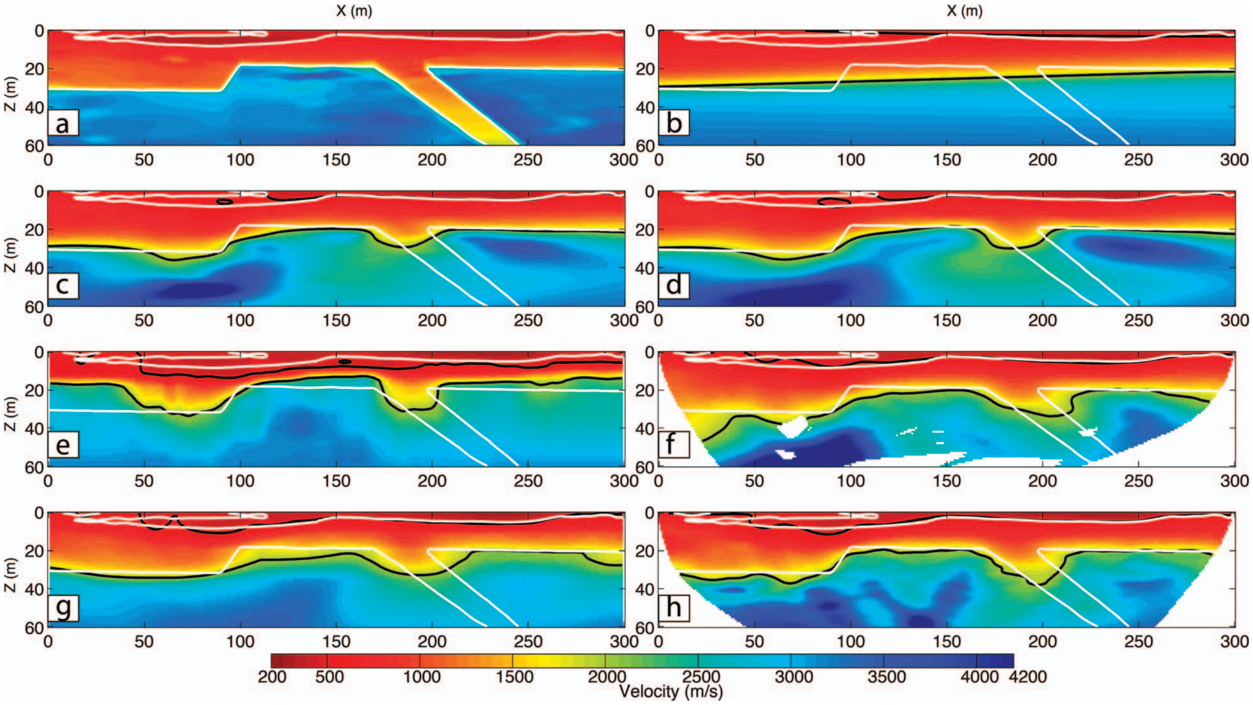

Figure 3. True and estimated models from this study and from SAGEEP 2011 blind test (Zelt *et al.,* 2013). a) True model. b) Starting model for IFTT and FDTT. c) IFTT model. d) FDTT model. Both IFTT and FDTT models provide an RMS misfit of 1 ms to the manually picked traveltimes. Models e) to h) are from the SAGEEP 2011 blind test. They are named after their index numbers in Zelt *et al.* (2013): e) V8, f) V14, g) V12, h) V10. Among the 14 models presented in Zelt *et. al.* (2013), V8 produces the smallest mean of the absolute difference from the true model, V14 produces the smallest mean of the relative difference, V12 produces the smallest standard deviation of the absolute difference, and V10 produces the smallest standard deviation of the relative difference. These four models provide RMS misfits of 1.4 ms, 1.6 ms, 1.2 ms, and 1.1 ms, respectively, to the synthetic traveltimes (Zelt *et. al.*, 2013). In each model, the black contours correspond to 500 m/s and 2,000 m/s. The white contours are from the true model for comparison.

same algorithm is used for forward modeling and inversion. Therefore, the inverted models in this paper represent ideal results one can expect from FWI.

Another commonly used pre-processing procedure for real data is time windowing to exclude later arrivals (*e.g.*, shear waves, surface waves) that are not modeled by visco-acoustic modeling (*e.g.*, Brenders and Pratt, 2007a). To honor the reality that only the early arrivals are typically used in FWI as a result of time windowing, an offset-dependent time window is applied to the modeled data in this study. The window is 50 ms at 0-m offset and linearly increases to 100 ms at 100-m offset, and is 100 ms beyond 100-m offset (Fig. 2). This window starts at the picked first-arrival time with a 10-ms cosine taper added before and after.

The outermost loop of the inversion is over frequency from low to high to mitigate the non-linearity of the seismic inverse problem. This implementation strategy is known as a multi-scale approach (Bunks *et al.*, 1995; Sirgue and Pratt, 2004). Effectively, low wavenumber, large-scale structure will first be introduced to the model updates, and then high wavenumber, fine-scale structure will improve the resolution in later iterations. The choice of the starting low frequency and stopping high frequency follows a trial and error procedure according to a visual assessment of 1) the spectra and signal-to-noise ratio of the real data, 2) the updated model for its overall geological sensibility and artifacts, and 3) the predicted data for their similarities with the real data (Gao *et al.*, 2006; Jaiswal *et al.*, 2009). In this study, we determined that the usable frequency range for FWI is 6 to 64 Hz. Below this range, the data have a poor consistency among different shots, which can be caused by the windowing operations; above this range, the data begin to introduce fine-scale artifacts especially to the shallow part of the model where there are relatively lower velocities and accordingly smaller seismic wavelengths. The data in the frequency domain are grouped with increasing frequency content. The first group is 6 Hz by itself, the second group is 8 and 10 Hz, and the rest of the groups each contain three frequency components without skipping or overlapping from 12 to 64 Hz, resulting in 11 groups in total. For the inversion of each group of frequencies, the source signature is first treated as an

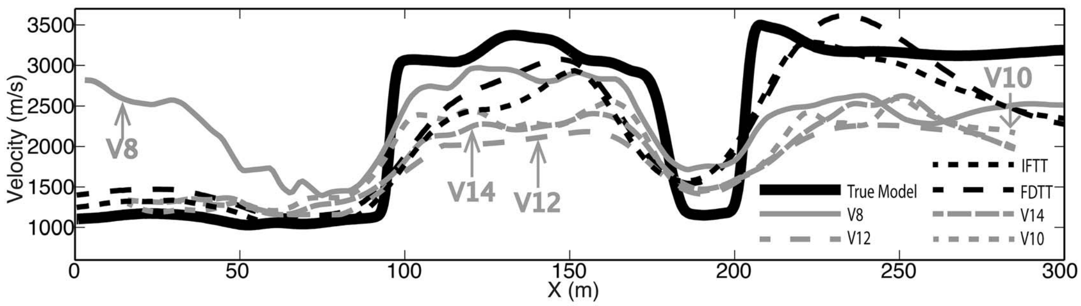

Figure 4. Comparison of a horizontal slice at Z = 25 m through the true model (Fig. 3(a)), IFTT model (Fig. 3(c)), FDTT model (Fig. 3(d)), and models from Zelt *et al.* (2013) (Figs. 3(e)-(h)).

unknown and is inverted from the observed data assuming a known velocity model provided by traveltime tomography. The source inversion is linear, *i.e.*, requires only one iteration, and produces a good match for both the amplitude and phase of the true source wavelet (Eq. 17 of Pratt (1999)). After that, the velocity model will be updated multiple times according to the stopping criterion assuming a known source signature. The source signature and the velocity model are iteratively updated as the frequency of each group increases.

The non-linear seismic waveform inversion problem is solved by a local decent method. The data misfit is defined by the L_2 norm of the data residual in the frequency domain so δ the objective function Φ is:

$$\Phi(\boldsymbol{m}) = \frac{1}{2}\,\delta \boldsymbol{d}^T \delta \boldsymbol{d}^*, \qquad (3)$$

where $\boldsymbol{m}$ is the model vector and $\delta \boldsymbol{d}$ is the waveform data residual vector. The superscript T represents matrix transpose, and the superscript * represents complex conjugate. The velocity model is iteratively updated according to the gradient of the data residual to minimize the misfit function. The data residual gradient gives the direction in which the misfit function decreases most for a given amount of change of the model. It is an iterative process and model updates stop when the misfit function diverges or when the largest model change among the entire grid is relatively small; less than 1% of the lowest velocity value in the model.

Results

Figures 3(c) and (d) show the IFTT and the FDTT models, both providing an RMS misfit of 1 ms to the picked data. A velocity contour of 2,000 m/s is used to interpret the boundary separating the sediments and bedrock (Zelt *et al.*, 2013). The shape of the boundary defines the bedrock offset and the dipping fault. Both the IFTT and the FDTT models give a smooth expression of the bedrock offset (centered at 95 m) and the shallow part of the fault (<30-m depth). For comparison, Figs. 3(e)–(h) present the best traveltime tomography models (V8, V14, V12 and V10) from Zelt *et al.* (2013) according to four different statistical measures.

The horizontal model slice at 25-m depth (Fig. 4) shows that the FDTT model overall matches the true model better than the IFTT model and the models from Zelt *et al.* (2013) in terms of a more accurate recovery of the absolute velocity values and a sharper velocity contrast defining the targeted geologic structures. This horizontal model slice captures the bedrock offset, a sharp velocity change from ~1,000 m/s to ~3,000 m/s between ~90–100 m lateral position, and the shallow part of the dipping fault, a ~20-m wide low-velocity interval between ~180–200 m lateral position. All of the estimated velocity models show these two velocity features smoothly. The FDTT, IFTT and V8 models present these two features more sharply with larger velocity contrasts. The FDTT and V8 models are better than the IFTT model with more accurate high velocities between ~100–170 m lateral position, which directly contributes to the definition of two key features in the model, the bedrock offset and the dipping fault. Elsewhere, the V8 model is inferior to the IFTT and FDTT models with generally less accurate velocity estimation, particularly an incorrect high-velocity feature at the left side of the model. The comparisons are not ideal in that the models from Zelt *et al.* (2013) were obtained from inverting calculated 100 Hz traveltimes from 101 shots, whereas the IFTT and FDTT models were obtained from picked traveltimes of the waveforms from 25 shots. Therefore, the differences between the TT models in Zelt *et al.* (2013) and the IFTT and FDTT models presented here are not merely the result of using different algorithms.

Taking the IFTT model (Fig. 3(c)) as the starting model, the IFTT-FWI-6Hz-64Hz model (Fig. 5(a)) is produced by starting FWI at 6 Hz and ending at 64 Hz. This model adds wavelength-scale structures that are weakly expressed or not visible in the starting model, including the low-velocity zone at 5-m depth defined by the 500 m/s contour and the deeper part of the dipping fault below 30-m depth, as seen in the 45-m depth slice

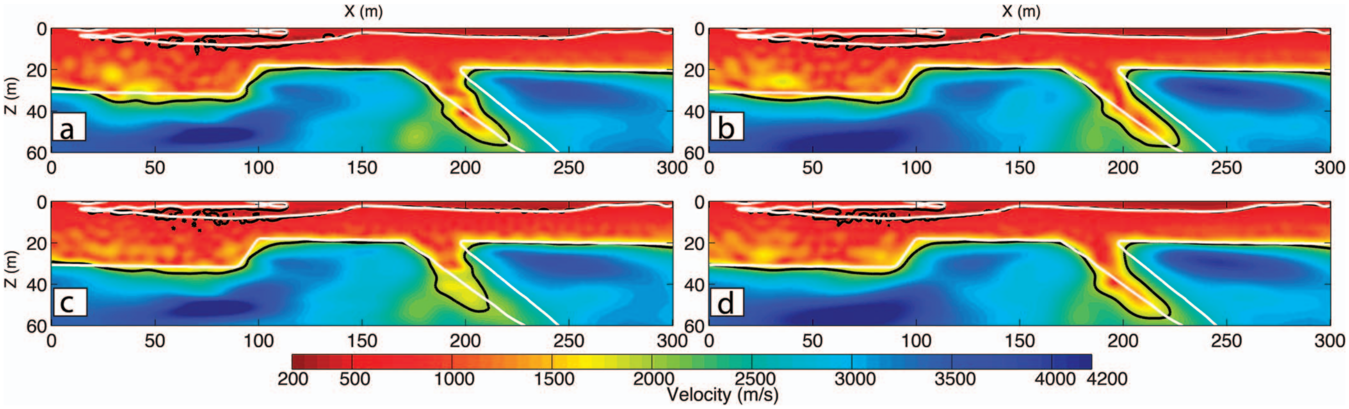

Figure 5. Full waveform inversion (FWI) estimated models. a) and c) are produced by taking IFTT model (Fig. 3(c)) as the starting model, and by starting the inversion at 6 Hz and 12 Hz, respectively. b) and d) are produced by taking FDTT model (Fig. 3(d)) as the starting model, and by starting the inversion at 6 Hz and 12 Hz, respectively. All inversions end at 64 Hz. In the text they are named a) IFTT-FWI-6Hz-64Hz model, b) FDTT-FWI-6Hz-64Hz model, c) IFTT-FWI-12Hz-64Hz model, and d) FDTT-FWI-12Hz-64Hz model. In each model, the black contours correspond to 500 m/s and 2,000 m/s. The white contours are from the true model for comparison.

in Fig. 6(b). The FWI model also improves the estimation of other features, *e.g.*, a steeper expression of the bedrock offset centered at ~95 m and a narrower expression of the shallow part of the dipping fault (Fig. 6(a)). The same observations apply to the comparison of the FDTT model (Fig. 3(d)) and the FDTT-FWI-6Hz-64Hz (Fig. 5(b)) model. Comparisons of the seismograms produced by the true model and the inverted models (Fig. 7) show a significantly better match of the seismic phases achieved by the FDTT-FWI-6Hz-64Hz model over the FDTT model. Compared with the FDTT model, the FDTT-FWI-6Hz-64Hz model achieves a 32% reduction in the waveform misfit function (Eq. 3). Both the qualitative and quantitative comparisons indicate a successful application of FWI.

Comparing the IFTT-FWI-6Hz-64Hz model (Fig. 5(a)) with the FDTT-FWI-6Hz-64Hz model (Fig. 5(b)), the latter shows a more continuous low-velocity zone at ~5-m depth, and a more accurate image of the deep part of the dipping fault (Fig. 6(b)). A realistic challenge for an application of FWI to real data is the lack of usable low frequency data because of noise, leading the inversion to converge to a local minimum (Bunks *et al.*, 1995). We simulate this situation by producing the IFTT-FWI-12Hz-64Hz model (Fig. 5(c)) and the FDTT-FWI-12Hz-64Hz model (Fig. 5(d)), which are the equivalents of the IFTT/FDTT-FWI-6Hz-64Hz models with a substitute of 12 Hz as the starting frequency. We observe degradation in image quality from starting the inversion at a higher frequency (compare Fig. 5(a) to 5(c), and 5(b) to 5(d)), for example, the low-velocity zone is less continuous and the image of the deep part of the dipping fault is less accurate. However, the FDTT-FWI-12Hz-64Hz model (Fig. 5(d)) is noticeably better than the IFTT-FWI-12Hz-64Hz model (Fig. 5(c)), and even slightly better than the IFTT-FWI-6Hz-64Hz model (Fig. 5(a)) in its continuous expression of the low-velocity zone. The FDTT-FWI-12Hz-64Hz model also a more accurate image of the deep part of the dipping fault. Comparing the FWI models with the TT models, even the IFTT-FWI-12Hz-64Hz model (Fig. 5(c)), the least accurate of the FWI results among the four, is still significantly better than any of the TT models (Figs. 3(c)–(h)).

Discussion

This study demonstrates the use of frequency-dependent traveltime tomography (FDTT) and full waveform inversion (FWI) for near-surface seismic velocity estimation. FDTT uses first-arrival times and takes the seismic data's frequency content into consideration to provide a starting model for FWI. FWI uses the waveforms of the early arrivals to improve the model resolution by adding wavelength-scale structure that is not in the traveltime model. In this study, the low-velocity zone, bedrock offset, and dipping fault are well imaged in all versions of the FWI models (Fig. 5) that would allow for direct geologic interpretation from the velocity model itself. These results confirm the suitability of using TT, and FDTT in particular, to provide the starting model for FWI. The importance of a good starting model for FWI has been widely discussed and confirmed by several researchers using FWI for different scales of geophysical studies (*e.g.*, Pratt *et al.*, 2002; Shah *et al.*, 2012; Wang *et al.*, 2014). The unique contribution of this paper is in proposing to use a new frequency-dependent

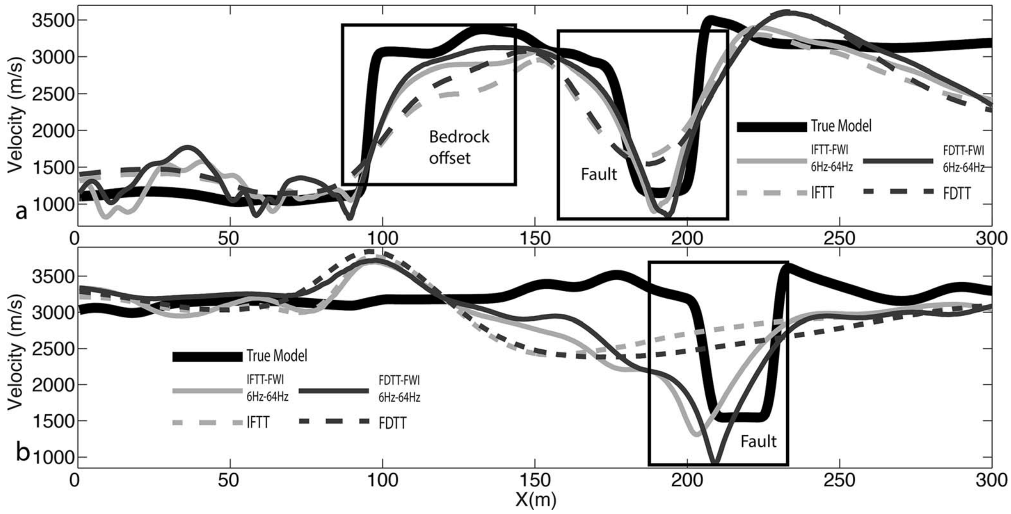

Figure 6. Comparison of horizontal slices through the true model (Fig. 3(a)), traveltime tomography estimated models (Figs. 3(c)–(d)), and full waveform inversion estimated models (Figs. 5(a)–(b)) at a) Z = 25 m and b) Z = 45 m. The black boxes highlight key features in the true model.

traveltime tomography to produce a better starting model than that produced by conventional ray-theory-based IFTT.

In this study, FDTT is superior to IFTT in two respects. Firstly, the FDTT model (Fig. 3(d)) more accurately estimates the magnitude of features, though it provides a similar scale of resolution as the IFTT model (Fig. 3(c)). This observation also applies to the model slice comparison (Fig. (4)) of the FDTT model with other TT models in Zelt *et al.* (2013), albeit this comparison is not ideal in that Zelt *et al.* (2013) used 100 Hz WDVS traveltimes from 101 sources, while this paper uses picked traveltimes from only 25 sources. Secondly, while both the IFTT and FDTT models (Figs. 3(c) and (d)) are appropriate starting models for FWI, FDTT provides a more suitable starting model in that the FDTT-FWI models reveal better velocity estimation compared with equivalent IFTT-FWI models that use the same frequency bandwidth of data (Fig. 5(b) compared with 5(a), 5(d) compared with 5(c)). More importantly, in a realistic situation where the low frequency data, in this case from 6 to 10 Hz, is not usable, the FDTT-FWI-12Hz-64Hz model (Fig. 5(d)) still recovers the targeted features well, *e.g.*, the deep part of the dipping fault, but the IFTT-FWI-12Hz-64Hz model (Fig. 5(c)) represents a significant degradation compared to the IFTT-FWI-6Hz-64Hz model (Fig. 5(a)).

Despite the potential for high resolution velocity estimation by FWI as shown in this study, application of FWI to real field data is challenging because of FWI's extreme nonlinearity. It also requires heuristic pre-processing steps, including pre-inversion amplitude matching to account for assumptions made in the wavefield modeling (Virieux and Operto, 2009), *e.g.*, 2-D acoustic modeling as in this study. FWI seeks the model with the best fit to the pre-processed data, and as such, there is always a risk of introducing unrealistic fine-scale structure. FWI uses heuristic criteria (*e.g.*, Jaiswal *et al.*, 2009) to stop the inversion iterations, including a visual comparison of the modeled and observed data (Fig. 7). As opposed to the difficulties of applying FWI to real data, no obstacle prevents the use of FDTT as long as first arrivals can be picked. In addition, traveltimes have a more linear relationship with seismic velocity than amplitudes. The FDTT model is obtained in a more objective manner using a misfit of the predicted and observed data quantified by a chi-square value taking the pick uncertainties into consideration (Zelt, 1999). It also honors Occam's principle that states that a minimum-structure solution containing only the model features required by the data is the best (Constable *et al.*, 1987). Although the development of a more objective workflow for the application of FWI is needed, we consider FDTT and other frequency-dependent/phase inversion techniques (*e.g.*, Ellefsen, 2009) to be a practical step forward over ray-theory-based TT for the non-expert practitioners dealing with near-surface seismic data.

Although we applied a realistic time window to honor the fact that FWI typically only makes use of the early arrivals when dealing with real data (Pratt, 1999), this study presents FDTT and FWI under nearly ideal circumstances since the data have no noise and the waveform data were calculated by the same algorithm used in FWI. Nevertheless, this paper shows what is possible with high-quality, realistic, near-surface seismic data using a combined strategy of FDTT and FWI.

The usable high frequency limit of FWI is not necessarily the high end of the spectrum, or even the

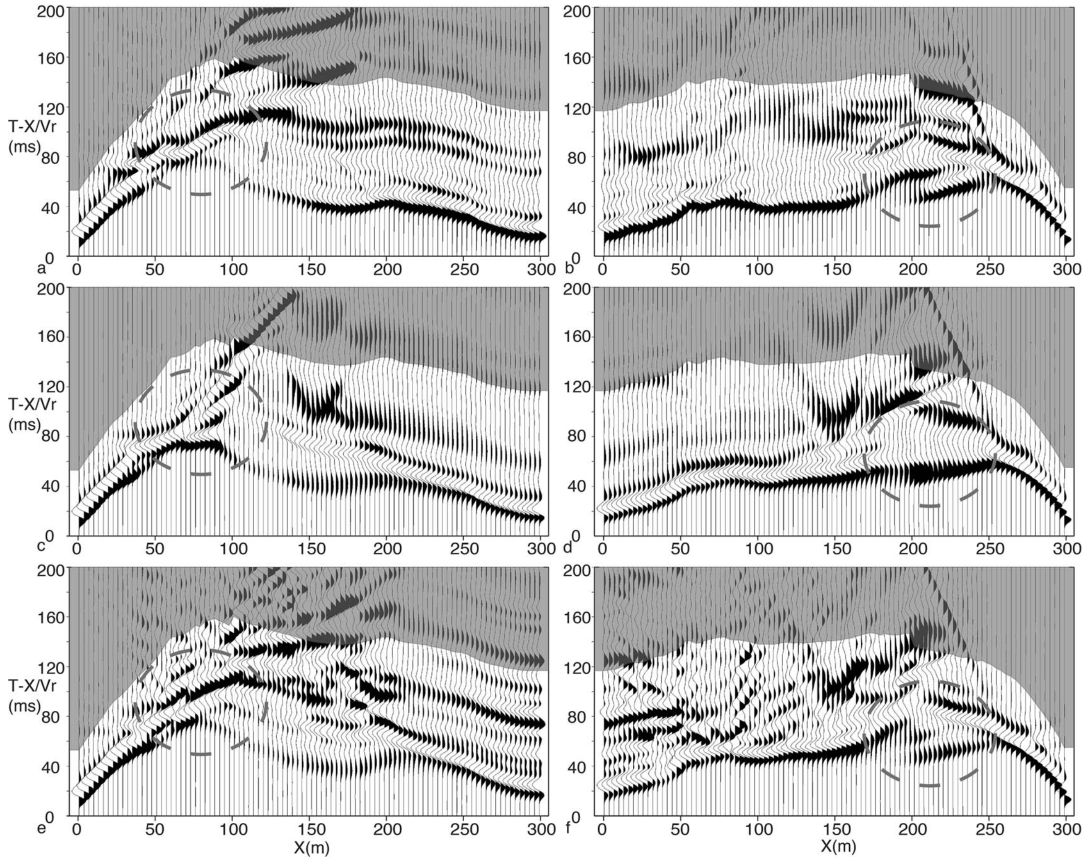

Figure 7. Representative synthetic acoustic seismograms from two end shots. a) and b) are calculated from the true model (Fig. 3(a)), c) and d) are calculated from the FDTT model (Fig. 3(d)), and e) and f) are calculated from the FDTT-FWI-6Hz-64Hz model (Fig. 5(b)). A reducing velocity (Vr) of 2,000 m/s is used to amplify subtle changes in the apparent velocities of both the near- and far-offset traces within the smallest possible time window. The seismic waveforms in the shaded areas were not used for waveform inversion as a result of the time window excluding later arrivals. Areas highlighted by the dashed gray ellipses are for detailed comparisons of the true and estimated model waveforms. Data are displayed with a low-pass filter of 70 Hz.

dominant frequency of the seismic data (*e.g.*, Jaiswal *et al.*, 2008), as is the case for this study. One factor that may influence the usable high frequency limit is the signal-to-noise ratio of each inverted frequency group. However, in this study with noise-free synthetic data, the frequency groups between the 20 dB points at 2 and 250 Hz, including those containing the dominant frequency and beyond, have effectively the same signal-to-noise ratio, contaminated only by a very small amount of numerical noise. Note, the relative energy differences between frequency groups, *i.e.*, being highest near the dominant frequency, are not important because the frequencies are not inverted simultaneously. Therefore, in this study, as with real data, the following three factors play a role in determining the high frequency limit. Firstly, the larger of the source and receiver spacing (the source spacing in this study) limits the highest possible frequency that can be used while avoiding spatial aliasing that can introduce spurious artifacts into the inverted model (Brenders and Pratt, 2007b). Secondly, a poor starting model can limit the highest possible frequency that can be used to avoid FWI converging to a local minimum, which can cause spurious artifacts in the inverted model (Bunks *et al.*, 1995; Pratt *et al.*, 2002). Finally, the time windowing operation excludes later parts of the waveforms that can reduce the consistency of the high frequency data, *e.g.*, a later-arriving seismic event may be included within the time window of some shot gathers, but outside the window of others. The effects of these factors are taken into consideration through empirical assessments during the inversions according to the criteria stated in the Methods section, and we determined that 64 Hz is the usable high frequency limit, lower than the dominant frequency of 80 Hz.

Conclusions

The workflow of applying FDTT followed by FWI to near-surface seismic refraction data shows the ability to achieve a velocity image with wavelength-scale features for direct interpretation of targeted structures. The velocity contours can be used to define the boundary between layers and zones of different rock properties for geologic interpretation. We used a laptop with a single processor to process the data from a realistically feasible seismic refraction survey to produce the FDTT and FWI models. The modest field acquisition effort and computational methods are accessible for solving near-surface problems in the environmental and engineering industries.

The results show that FDTT better estimates velocity than IFTT, and the FDTT velocity model serves as a more suitable starting model for FWI. FDTT uses frequency information in both the forward and inversion modeling steps (Zelt and Chen, 2016). Its improvements stem from the calculation of frequency-dependent traveltimes, naturally resulting in frequency-dependent sensitivity kernels. This is fundamentally different from traveltime tomography methods that adopt a frequency-dependent kernel for the inversion without forward calculating a frequency-dependent traveltime (*e.g.*, Watanabe *et al.*, 1999; Liu *et al.*, 2009).

Acknowledgments

This research was funded by National Science Foundation grant EAR-1056073 and Department of Energy grant DE-FG07-97ER14827. The authors would like to thank Gerhard Pratt for providing the FWI code. The authors are also grateful to Priyank Jaiswal, Fuchun Gao, and Geoff Chambers for help with applying FWI. Comments by William Doll, Zhangshuan Hou, and an anonymous reviewer helped to clarify the text.

References

Adamczyk, A., Malinowski, M., and Malehmir, A., 2014, High-resolution near-surface velocity model building using full-waveform inversion—A case study from southwest Sweden: Geophysical Journal International, **197**(3) 1693–1704.

Baumann-Wilke, M., Bauer, K., Schovsbo, N.H., and Stiller, M., 2012, P-wave traveltime tomography for a seismic characterization of black shales at shallow depth on Bornholm, Denmark: Geophysics, **77**(5) EN53–EN60.

Brenders, A.J., and Pratt, R.G., 2007a, Full waveform tomography for lithospheric imaging: Results from a blind test in a realistic crustal model: Geophysical Journal International, **168**(1) 133–151.

Brenders, A.J., and Pratt, R.G., 2007b, Efficient waveform tomography for lithospheric imaging: Implications for realistic, two-dimensional acquisition geometries and low-frequency data: Geophysical Journal International, **168**(1) 152–170.

Bunks, C., Saleck, F.M., Zaleski, S., and Chavent, G., 1995, Multiscale seismic waveform inversion: Geophysics, **60**(5) 1457–1473.

Constable, S.C., Parker, R.L., and Constable, C.G., 1987, Occam's inversion: A practical algorithm for generating smooth models from electromagnetic sounding data: Geophysics, **52**(3) 289–300.

Doll, W.E., Miller, R.D., and Xia, J., 1998, A noninvasive shallow seismic source comparison on the Oak Ridge Reservation, Tennessee: Geophysics, **63**(4) 1318–1331.

Ellefsen, K.J., 2009, A comparison of phase inversion and traveltime tomography for processing near-surface refraction traveltimes: Geophysics, **74**(6) WCB11–WCB24.

Gao, F., Levander, A., Pratt, R.G., Zelt, C.A., and Fradelizio, G.L., 2007, Waveform tomography at a groundwater contamination site: Surface reflection data: Geophysics, **72**(5) G45–G55.

Gao, F., Levander, A.R., Pratt, R.G., Zelt, C.A., and Fradelizio, G.L., 2006, Waveform tomography at a groundwater contamination site: VSP-surface data set: Geophysics, **71**(1) H1–H11.

Hole, J.A., and Zelt, B.C., 1995, 3-D finite-difference reflection traveltimes: Geophysical Journal International, **121**(2) 427–434.

Jaiswal, P., Zelt, C.A., Bally, A.W., and Dasgupta, R., 2008, 2-D traveltime and waveform inversion for improved seismic imaging: Naga Thrust and Fold Belt, India: Geophysical Journal International, **173**(2) 642–658.

Jaiswal, P., Zelt, C.A., Dasgupta, R., and Nath, K.K., 2009, Seismic imaging of the Naga thrust using multiscale waveform inversion: Geophysics, **74**(6) WCC129–WCC140.

Liu, Y., Dong, L., Wang, Y., Zhu, J., and Ma, Z., 2009, Sensitivity kernels for seismic Fresnel volume tomography: Geophysics, **74**(5) U35–U46.

Pelton, J.R., 2005, Near-surface seismology; surface-based methods: *in* Near-Surface Geophysics, Butler D.K. (ed.), Investigations in Geophysics, No. 13, Society of Exploration Geophysicists, Tulsa, OK, 219–263.

Pratt, R.G., 1999, Seismic waveform inversion in the frequency domain, Part 1: Theory and verification in a physical scale model: Geophysics, **64**(3) 888–901.

Pratt, R.G., Gao, F., Zelt, C.A., and Levander, A.R. (2002). The limits and complementary nature of traveltime and waveform tomography: Journal of Conference Abstracts, **7**(2) 181–182.

Pratt, R.G., Shin, C., and Hick, G.J., 1998, Gauss–Newton and full Newton methods in frequency–space seismic waveform inversion: Geophysical Journal International, **133**(2) 341–362.

Ramachandran, K., Bellefleur, G., Brent, T., Riedel, M., and Dallimore, S., 2011, Imaging permafrost velocity structure using high resolution 3D seismic tomography: Geophysics, **76**(5) B187–B198.

Ravaut, C., Operto, S., Improta, L., Virieux, J., Herrero, A., and Dell'Aversana, P., 2004, Multiscale imaging of complex structures from multifold wide-aperture seismic data by frequency-domain full-waveform tomography: Application to a thrust belt: Geophysical Journal International, **159**(3) 1032–1056.

Rohdewald, S., 2014, Optimized interpretation of SAGEEP 2011 blind refraction data with Fresnel volume tomography and plus-minus refraction: in Proceedings: Symposium on the Application of Geophysics to Engineering and Environmental Problems, 374–382.

Shah, N., Warner, M., Nangoo, T., Umpleby, A., Stekl, I., Morgan, J., and Guasch, L., 2012, Quality assured full-waveform inversion: Ensuring starting model adequacy: in Expanded Abstracts: 82nd Annual International Meeting, Society of Exploration Geophysics, 1228–1231.

Sirgue, L., and Pratt, R.G., 2004, Efficient waveform inversion and imaging: A strategy for selecting temporal frequencies: Geophysics, **69**(1) 231–248.

Smithyman, B., Pratt, R.G., Hayles, J., and Wittebolle, R., 2009, Detecting near-surface objects with seismic waveform tomography: Geophysics, **74**(6) WCC119–WCC127.

Steeples, D.W., 2001, Engineering and environmental geophysics at the millennium: Geophysics, **66**(1) 31–35.

Stoyer, C., 2012, Interpreting Colin Zelt's "Shootout" Seismic Refraction Data Set Using the Generalized Reciprocal Method: in Proceedings: Symposium on the Application of Geophysics to Engineering and Environmental Problems, 470–478.

Vidale, J., 1988, Finite-difference calculation of travel times: Bulletin of the Seismological Society of America, **78**(6) 2062–2076.

Virieux, J., and Operto, S., 2009, An overview of full-waveform inversion in exploration geophysics: Geophysics, **74**(6) WCC1–WCC26.

Wang, H., Singh, S.C., and Calandra, H., 2014, Integrated inversion using combined wave-equation tomography and full waveform inversion: Geophysical Journal International, **198**(1) 430–446.

Watanabe, T., Matsuoka, T., and Ashida, Y., 1999, Seismic traveltime tomography using Fresnel volume approach: in Expanded Abstracts: 69th Annual International Meeting, Society of Exploration Geophysics, 1402–1405.

Zelt, C.A., 1999, Modelling strategies and model assessment for wide-angle seismic traveltime data: Geophysical Journal International, **139**(1) 183–204.

Zelt, C.A., and Barton, P.J., 1998, Three-dimensional seismic refraction tomography: A comparison of two methods applied to data from the Faeroe Basin: Journal of Geophysical Research: Solid Earth (1978–2012), 103(B4) 7187–7210.

Zelt, C.A., and Chen, J., 2016, Frequency-dependent traveltime tomography for near-surface seismic refraction data: Geophysical Journal International, submitted.

Zelt, C.A., Haines, S., Powers, M.H., Sheehan, J., Rohdewald, S., Link, C., Hayashi, K., Zhao, D., Zhou, H., Burton, B.L., Petersen, U.K., Bonal, N.D., and Doll, W.E., 2013, Blind test of methods for obtaining 2-D near-surface seismic velocity models from first-arrival traveltimes: Journal of Environmental and Engineering Geophysics, **18**(3) 183–194.

Zelt, C.A., and Smith, R.B., 1992, Seismic traveltime inversion for 2-D crustal velocity structure: Geophysical Journal International, **108**(1) 16–34.

Zhao, Z., and Xu, J., 2010, Geological structure investigation of shallow layers by the explosion seismic survey tomographic technique: Journal of Environmental and Engineering Geophysics, **15**(1) 21–28.